A Resistor-Based Temperature Sensor With a 0.13 pJ·K^2 Resolution FoM

Sining Pan, *Student Member, IEEE*, Yanquan Luo, Saleh Heidary Shalmany, *Student Member, IEEE*, and Kofi A. A. Makinwa, *Fellow, IEEE*

Abstract—This paper describes a high-resolution energy-efficient CMOS temperature sensor, intended for the temperature compensation of MEMS/quartz frequency references. The sensor is based on silicided poly-silicon thermistors, which are embedded in a Wien-bridge RC filter. When driven at a fixed frequency, the filter exhibits a temperature-dependent phase shift, which is digitized by an energy-efficient continuous-time phase-domain delta-sigma modulator. Implemented in a 0.18-μm CMOS technology, the sensor draws 87 μA from a 1.8 V supply and achieves a resolution of 410 μK$_{rms}$ in a 5-ms conversion time. This translates into a state-of-the-art resolution figure-of-merit of 0.13 pJ $\cdot$ K^2. When packaged in ceramic, the sensor achieves an inaccuracy of 0.2 °C (3σ) from −40 °C to 85 °C after a single-point calibration and a correction for systematic nonlinearity. This can be reduced to ±0.03 °C (3σ) after a first-order fit. In addition, the sensor exhibits low 1/f noise and packaging shift.

Index Terms—Calibration, CMOS temperature sensor, continuous-time phase-domain delta-sigma modulator (PD$\Delta\Sigma$M), energy efficiency, resistor-based sensor, temperature compensation.

I. Introduction

INTEGRATED temperature sensors are widely used for the temperature compensation of frequency references [1]–[7]. This is a demanding application, as it requires sensors that can simultaneously achieve high resolution, high energy efficiency, and high stability. High resolution is needed to prevent the temperature sensor's noise from increasing the frequency reference's jitter [7]. High energy efficiency is needed to minimize the sensor's contribution to the reference's total energy budget. Last, but not least, high stability is required to guarantee the reference's long-term stability over temperature. Furthermore, the sensor should be CMOS-compatible so that it can be co-integrated with the rest of the frequency reference's electronics.

The temperature dependencies of various CMOS-compatible devices, such as bipolar junction transistors (BJTs)

[8]–[10], MOSFETs [11], [12], resistors [1]–[6], [13], and electrothermal filters [14], [15] have all been used as the basis for integrated temperature sensors. MEMS resonators have also been used to realize temperature sensors with excellent resolution and energy efficiency [7]. However, they are fabricated in non-CMOS processes, leading to two-die systems, greater complexity, and increased cost. According to a survey of smart temperature sensors [16], resistor-based sensors are currently the most energy-efficient class of CMOS temperature sensors. As expressed by their resolution figure-of-merit (FoM) [16], they can be an order of magnitude more efficient than their BJT-based counterparts. Furthermore, they can achieve higher (sub-mK) resolution [1].

The resolution and energy efficiency of a resistor-based temperature sensor are determined by the temperature coefficient (TC) of its sensing resistor and the noise of its readout electronics. In [3], poly resistors were used, while in [4], both poly and diffusion resistors were used. In both cases, however, their resolution was limited by the thermal [3], or 1/f [4], noise of the readout electronics. The designs in [5] and [13] used N-well and silicided resistors, respectively, which both have larger TCs (∼0.3%/°C) than diffusion or poly resistors. However, their resolution was still limited by the readout electronics' thermal [5], or quantization [13] noise.

In this paper, we describe the design of a high-resolution, energy-efficient temperature sensor based on a thermistor-embedded Wien-bridge (WB) *RC* filter. When driven at a fixed frequency, the bridge exhibits a temperature-dependent phase shift. Since the capacitors in a CMOS process are comparatively stable, this temperature dependence will be mainly determined by the resistor's TC. This phase shift can then be digitized by a high-resolution ADC based on an energy-efficient continuous-time phase-domain delta-sigma modulator (PD$\Delta\Sigma$M). The WB sensor achieves a resolution of 410 μK$_{rms}$ in a 5-ms conversion time, and a resolution FoM of 0.13 pJ·K^2. To study the impact of process spread and mechanical stress on sensor inaccuracy, samples from two different batches, as well as samples packaged in both ceramic and plastic, were characterized.

The rest of this paper is organized as follows. Section II reviews the properties of different resistors in CMOS processes and then describes the characteristics of the WB sensor. Section III is devoted to the design of an energy-efficient continuous-time PD$\Delta\Sigma$M. Measurement results and a comparison with the state of the art are described in Section IV, and finally, conclusions are presented in Section V.

TABLE I
CHARACTERISTICS OF THE RESISTORS AVAILABLE IN CMOS PROCESSES

Resistor type	Metal	Diffusion	N-well	Poly	Silicided diffusion	Silicided poly
Temperature coefficient	Large	Medium	Large	Medium or Small	Large	Large
2nd-order Temperature coefficient	Medium	Medium	Large	Medium	Small	Small
Sheet resistance	Very Small	Large	Large	Large	Medium	Medium
Supply dependency	Small	Medium	Large	Small	Small	Small
1/f noise	No	No	No	Large	Small	Small
Stress sensitivity	Small	Large	Large	Medium	Small	Small

II. RESISTOR-BASED SENSORS

A. Characteristics of CMOS Resistors

In CMOS processes, many resistors are available: metal resistors, diffusion resistors, poly-silicon (poly) resistors, and silicided resistors. The relevant characteristics of these resistors are summarized in Table I. To achieve high resolution, high energy efficiency, and high stability, a temperature-sensing resistor should have a large TC, low 1/f noise, and a stable resistance, i.e., low voltage dependence and low stress sensitivity.

Metal resistors are quite stable, and have large TCs, typically ranging from 0.3% to 0.4%/°C. However, their sheet resistance is very low (<0.1 $\Omega/\square$ in the process used), resulting in either large chip area or high power consumption. Poly-silicon resistors have smaller TCs (<0.15%/°C in the process used) and exhibit more 1/f noise [17]. The resistance of diffusion resistors depends on doping level, and on the reverse-bias voltage between them and the substrate (or well diffusion). Due to their low doping levels, this is particularly an issue for N-well resistors, which, however, can have TCs comparable to that of metal resistors.

Two other resistor types are available: silicided poly resistors and silicided diffusion resistors. Silicide is a highly conductive silicon–metal alloy and so the characteristics of such resistors are in between those of metal and (poly-)silicon resistors. Compared to the latter, they have a relatively large TC (~0.3%/°C), a more linear temperature dependence and lower 1/f noise [17]. However, their sheet resistance is much lower (a few ohms/square). They also have low voltage dependence and low stress sensitivity, and are quite stable, showing no electrical degradation (e.g., hysteresis), even after being heated up to 500 °C [18].

From Table I, it would seem that of the available resistors in standard CMOS processes, silicided resistors are the best choice for use in high-performance temperature sensors. In the chosen process (TSMC 0.18-μm CMOS), both silicided

diffusion resistors and silicided poly resistors are available. However, the former spread more, and have larger parasitic capacitances. The silicided p-poly resistor (s-p-poly resistor) is less voltage dependent than the silicided n-poly one, and so was chosen as the main temperature-sensing element in this paper.

B. Wien-Bridge Temperature Sensors

Apart from a sensing element, a resistor-based temperature sensor also requires a reference impedance, which has a stable, preferably near zero TC. According to Section II-A, however, such resistors are not available in standard CMOS processes. Alternatively, the very low TC (~10 ppm/°C [19]) of metal–insulator–metal (MIM) capacitors can be exploited to realize a stable reference impedance by driving them at a fixed reference frequency, as is the case in a WB sensor.

The circuit diagram of a WB RC filter is shown in Fig. 1(a). It is a second-order bandpass filter, whose voltage amplitude and phase transfer functions can be written as

$$H(j\omega) = \frac{RCj\omega}{1 - R^2C^2\omega^2 + 3RCj\omega} \tag{1}$$

$$\varphi_{WB}(\omega) = -\tan^{-1}\left(\frac{R^2C^2\omega^2 - 1}{3RC\omega}\right). \tag{2}$$

Its Bode plot is shown in Fig. 1(b), where the frequency axis is normalized by $f_0 = 1/(2\pi RC)$.

For a fixed driving frequency f_{drive}, the phase shift of the WB will be determined by its resistors and capacitors. Since the TC of MIM capacitors is quite low, the temperature dependence of this phase shift will be mainly determined by that of the resistors. With s-p-poly resistors, this will vary from about −7° to 10° over the industrial temperature range (−40 °C to 85 °C). As shown in Fig. 1(c), this phase shift can be determined by measuring either the voltage across the output resistor 2R(T) or the current flowing through it, In this paper, the former method is referred to as the voltage readout scheme, and the latter as the current readout scheme.
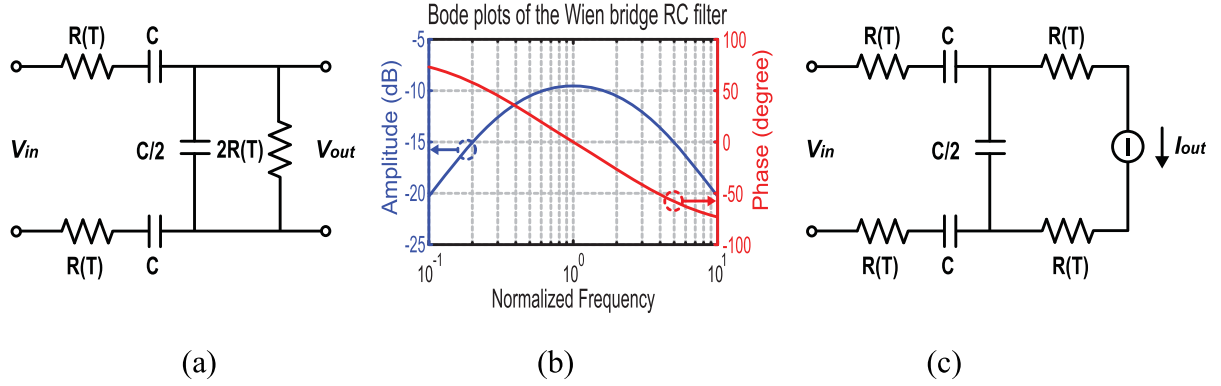
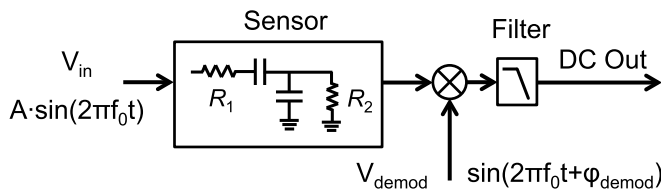Fig. 1.   (a) WB sensor, voltage readout scheme. (b) Bode plots. (c) WB sensor, current readout scheme.

Fig. 2.   Phase detection of a WB sensor.

C. Resolution and Energy Efficiency

An ideal phase detection model based on synchronous demodulation, shown in Fig. 2, can be used to estimate the achievable temperature-sensing resolution and the resolution FoM of the WB sensor. For simplicity, both the driving and the demodulating signals are assumed to be sine waves with the same frequency, but different phases: $V_{in} = A \cdot \sin(2\pi f_0 t)$ and $V_{demod} = \sin(2\pi f_0 t + \varphi_{demod})$, where $f_0 = 1/(2\pi RC)$, $\varphi_{demod} = 90°$ (orthogonal), and A is the amplitude of the driving signal. The resolution of the WB sensor can then be derived by comparing the levels of the noise and the temperature dependent dc signal present at the output of the low-pass filter. The demodulating signal is assumed to be noise-free, and thus its amplitude does not affect the sensor's resolution.

First, we assume a voltage readout scheme. Under the orthogonal sine wave assumption, the sensitivity of the demodulator's dc output to temperature can be expressed as

$$S_{WB,v} = \frac{dV_{dc}}{dT} = \frac{dV_{dc}}{d\varphi_{WB}} \cdot \frac{d\varphi_{WB}}{dT} = \frac{A}{6} \cdot \frac{2\alpha}{3} = \frac{A\alpha}{9} \quad (3)$$

where α is the TC of the sensing resistors. At the driving frequency f_0, the noise spectrum densities of R_1 and R_2 in Fig. 2 before demodulation are $v_{n,r1} = (4kTR/9)^{1/2}$ and $v_{n,r2} = (8kTR/9)^{1/2}$, respectively. After demodulation, the noise power will be quartered, as the power of the unity-amplitude demodulation sine wave is 0.5 and only half of the noise power will be demodulated to dc. Given a conversion time of t_{conv}, the amplitude of the output voltage noise becomes

$$\bar{V}_n = \sqrt{v_{n,r1}^2 + v_{n,r2}^2} \cdot \sqrt{\frac{1}{2t_{conv}}} \cdot \sqrt{\frac{1}{4}} = \sqrt{\frac{kTR}{6t_{conv}}}. \quad (4)$$

By combining (3) and (4), the resolution of this single-ended WB sensor can be expressed as

$$\Delta T_{v,se} = \frac{\bar{V}_n}{S_{WBv}} = \frac{3}{A\alpha}\sqrt{\frac{3kTR}{2t_{conv}}}. \quad (5)$$

For a differential WB sensor, however, this resolution can be improved by $\sqrt{2}$ due to the doubled noise power and the quadrupled signal power, that is

$$\Delta T_{v,diff} = \frac{3}{A\alpha}\sqrt{\frac{3kTR}{t_{conv}}}. \quad (6)$$

In the current readout scheme, however, the noise contribution of R_2 is less attenuated than in the voltage readout scheme, and thus the temperature resolution is lower. In the case of a differential WB sensor it is given by

$$\Delta T_{i,diff} = \frac{3}{A\alpha}\sqrt{\frac{3kTR}{2t_{conv}}}. \quad (7)$$

When driven at its center frequency f_0, the power consumed by the differential bridge is $A^2/(3R)$. By combining this with (7), the sensor's FoM can be calculated. In the voltage readout scheme, $FoM_{v,WB} = 9kT/(4\alpha^2)$; while in the current readout scheme, $FoM_{i,WB} = 9kT/(2\alpha^2)$. Interestingly, these expressions are independent of other design parameters such as resistance, capacitance, supply voltage, or conversion time.

In the actual design, the WB sensor is implemented with $R = 32$ kΩ, $C = 10$ pF, and $f_{drive} = 500$ kHz. Although the voltage readout scheme is more energy efficient, the current readout scheme can be easily connected to a virtual ground, thus simplifying the readout circuitry [2]. From (3), with $t_{conv} = 5$ ms and $A = 0.9$ V (1.8-V supply voltage), a WB based on an s-p-poly resistor can achieve a temperature-sensing resolution of 230 μK$_{rms}$. The corresponding $FoM_{i,WB}$ is then 2.3 fJ·K^2. It should be noted that this does not take into account the noise and power consumption of the readout electronics, and it assumes that the sensor is driven and demodulated by sine waves.
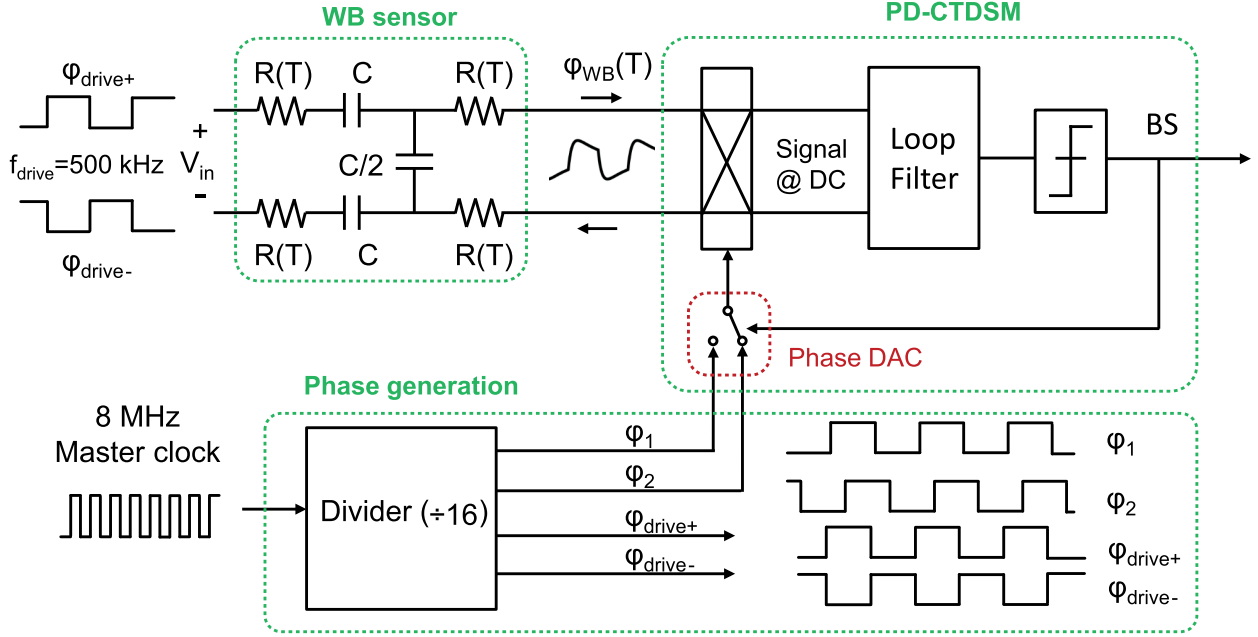
Fig. 3.   Simplified block diagram of the proposed temperature sensor.

III. ARCHITECTURE AND READOUT CIRCUIT IMPLEMENTATION

A. System-Level Design

The block diagram of the proposed temperature sensor is shown in Fig. 3. To simplify the driving circuitry and minimize its energy consumption, the WB is driven by complementary square waves, instead of by sine waves. The driving signals, $\varphi_{\text{drive}+}$ and $\varphi_{\text{drive}-}$, at $f_{\text{drive}} = 500$ kHz, are derived from an 8-MHz external master clock by a divide-by-16 circuit. For high resolution, a continuous-time PD$\Delta\Sigma$M is adopted to digitize the phase $\varphi_{\text{WB}}(T)$ of the WB's output current. For simplicity and linearity, it employs a single-bit quantizer. The two square-wave phase references of the PD$\Delta\Sigma$M, $\varphi_1 = 67.5°$ and $\varphi_2 = 112.5°$, are also generated by the divider circuitry. Their phase difference of 45° is chosen in order to accommodate the spread of the WB's resistors and capacitors, and hence in $\varphi_{\text{WB}}(T)$.

The PD$\Delta\Sigma$M first down-converts $\varphi_{\text{WB}}(T)$ to dc by multiplying it by a phase reference at the same frequency ($f_{\text{demod}} = f_{\text{drive}}$). Depending on the chosen references φ_1 or φ_2 of the phase DAC, the multiplier's dc output is either positive or negative [14]. The multiplier's output is integrated by the loop filter, and then quantized. In a negative feedback loop, the quantizer toggles the reference phases such that the loop filter's average dc input is zero. The average of the output bit stream is therefore a digital representation of $\varphi_{\text{WB}}(T)$.

In contrast to a previous design, which was based on a first-order modulator [2], this design employs a second-order modulator to achieve sub-mK resolution in a short (5 ms) conversion time. As shown in Fig. 4, it employs a feedforward topology [20], which requires only one feedback DAC, and also reduces the swing in the loop filter.
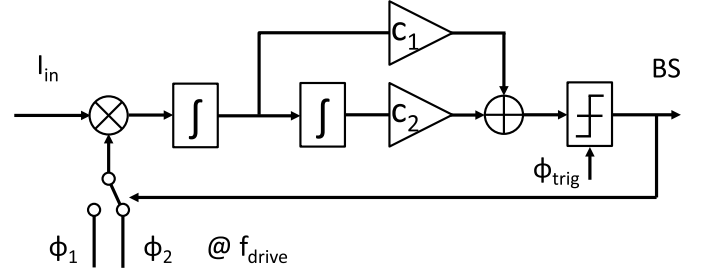
Fig. 4.   Block diagram of the continuous-time PD$\Delta\Sigma$M.
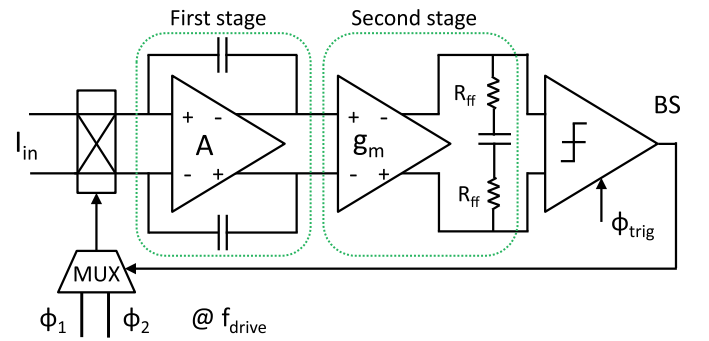
Fig. 5.   Circuit diagram of the continuous-time PD$\Delta\Sigma$M.

B. Circuit Implementation

Fig. 5 shows the circuit diagram of the continuous-time PD$\Delta\Sigma$M. The demodulator is realized by controlling the direction of the input current flow, i.e., by chopping the input current with bit stream-dependent phases φ_1 and φ_2. To establish a low-impedance virtual ground at the input of the ADC, the first stage consists of an active integrator, while, for simplicity, the second stage consists of a gm-C integrator. The feedforward coefficient c_1 (Fig. 4) is realized by the
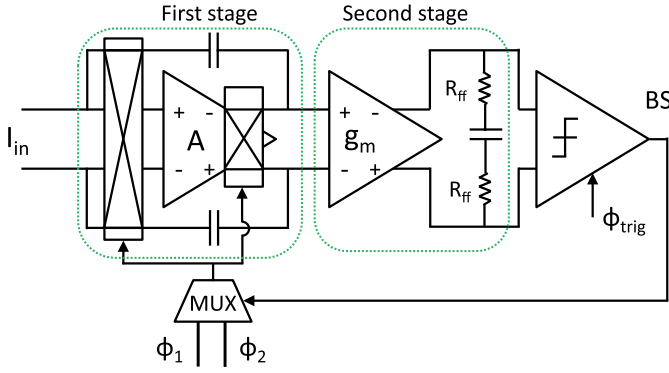
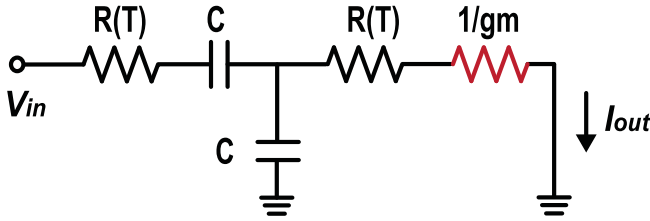Fig. 6. Circuit diagram of the continuous-time PDΔΣM, with merged chopper.

Fig. 7. Additive resistance on the output resistor of WB sensor when using an OTA-based first stage.

introduction of R_{ff} in series with the integration capacitor of the second stage. Its output is sampled at f_{drive} by a comparator, which is triggered at $\varphi_{trig} = 135°$.

To suppress its $1/f$ noise, the opamp of the first stage is chopped. By choosing the chopping frequency f_{chop} the same as f_{demod}, the input chopper and the input demodulator can be merged into a single chopper in series with the integration capacitors, as shown in Fig. 6. This chopper merging technique [14] simplifies the required control logic and minimizes errors due to charge injection mismatch.

In principle, the first-stage amplifier can be implemented as an energy-efficient single-stage operational transconductance amplifier (OTA). However, the input impedance of the resulting integrator is then approximately 1/gm, where gm is the OTA's transconductance. As shown in Fig. 7, this resistance loads the WB, thus altering $\varphi_{WB}(T)$ and degrading its temperature-sensing accuracy. For example, with the chosen s-p-poly resistors, a 10% variation on a nominal gm of 1 mS ($I_d \sim 50~\mu A$, or 4 × larger than the maximum output current of the WB) will translate into a temperature-sensing error of more than 0.5 °C.

In a two-stage amplifier, the input stage does not need to provide the output current. This helps to reduce its input swing and hence the input impedance of the first integrator, which in turns results in less temperature-sensing error. For simplicity, and to avoid the need for Miller compensation capacitors, the gain of the output stage should not be large, so that the pole formed by the output stage is well beyond the unity-gain frequency of the amplifier. In this paper, the first stage is a two-stage opamp consisting of a telescopic gm stage followed by two PMOS source followers, as shown in Fig. 8. The common-mode feedback of the gm stage is achieved by
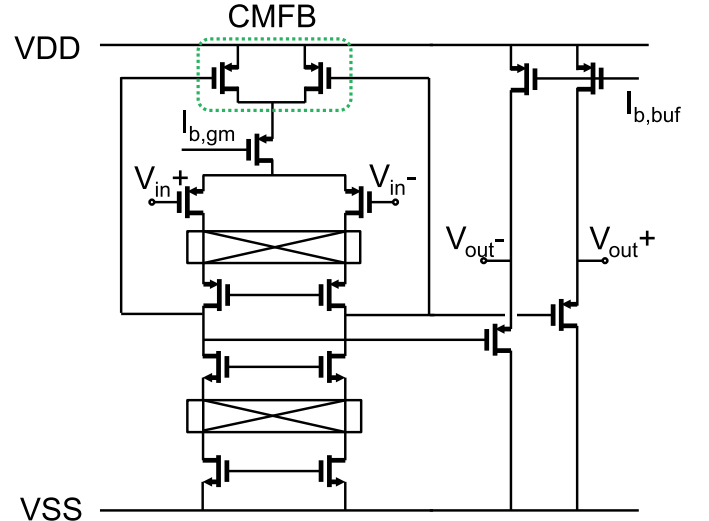

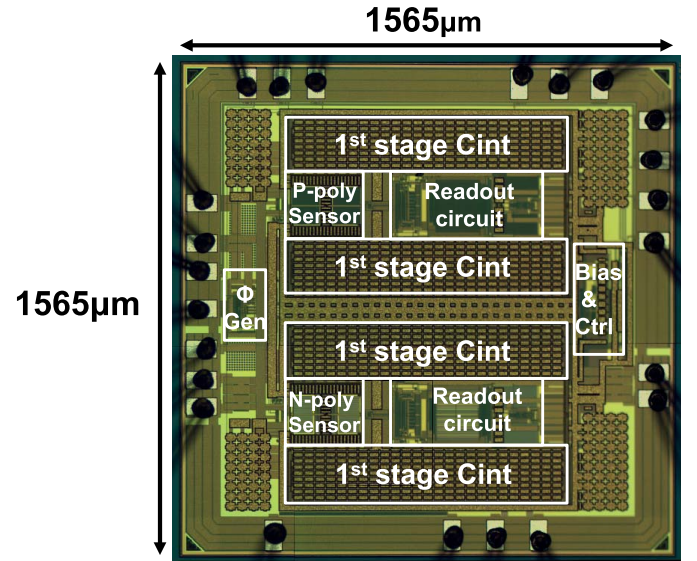Fig. 8. Schematic of the opamp in the first stage.

Fig. 9. Micrographs of the WB sensor chip.

two PMOS transistors in their triode region. The tail current of the telescopic gm, which is 16 μA at room temperature, is optimized for low noise and power consumption. The source followers' bias current (20 μA/branch at room temperature) is chosen to handle the WB's peak current (11 μA at room temperature, 16 μA at −40 °C). The opamp's $1/f$ noise has a corner frequency of about 15 kHz, and so is effectively cancelled by chopping at 500 kHz. To limit the first-stage's output swing (which includes chopper ripple) and thus to relax the design of the gm-C second stage, the integration capacitor of the first stage is made quite large (180 pF each). The gm-C second stage is built around a telescopic OTA with source degenerated input pairs, which achieves a good balance between energy efficiency and linearity. It draws 4 μA, which is less than 10% of that of the first stage.

IV. MEASUREMENT RESULTS

The sensor is fabricated in a standard 0.18-μm CMOS technology, and the chip micrograph is shown in Fig. 9.

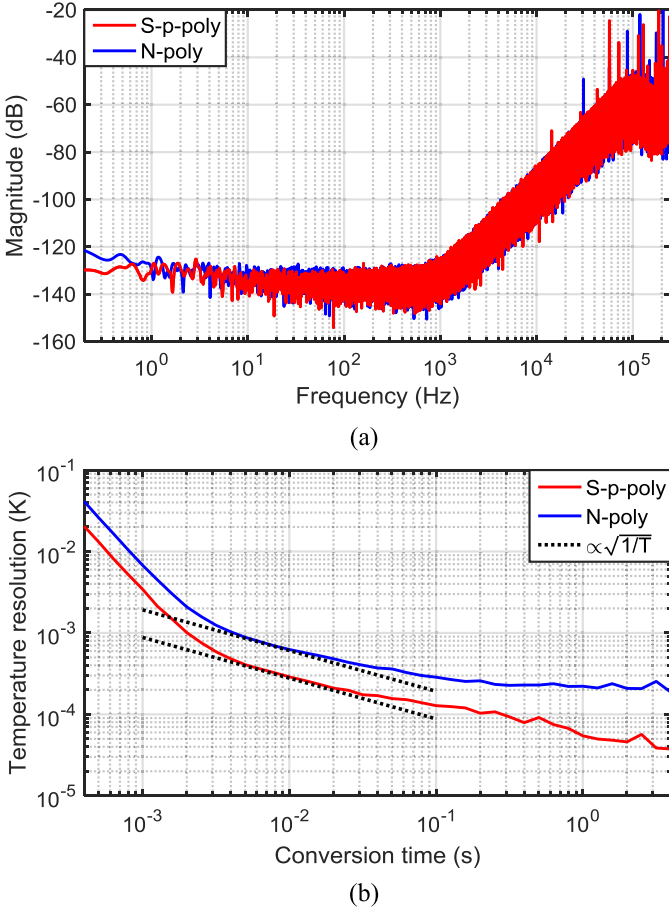Fig. 11. Normalized resistance versus bit-stream average of WB sensors.

Fig. 10. (a) Power spectral density of the output bit stream and (b) temperature resolution versus conversion time of both WB sensors.

For flexibility, a sinc² decimation filter is implemented off-chip. Each sample contains two different temperature sensors: one with silicided p-poly (s-p-poly) resistors, and for the sake of comparison, the other with non-silicided n-poly resistors. These two co-integrated sensors share the same constant-gm biasing and phase generation circuits. Each sensor occupies an active die area of 0.72 mm², about 40% of which is consumed by the first integrator's capacitors (2×180 pF). Each sensor draws 87 μA from a 1.8-V power supply including the readout circuits. At room temperature, dc supply sensitivities of -0.17 °C/V (s-p-poly bridge) and 0.34 °C/V (n-poly bridge) were observed for supply voltages ranging from 1.6 to 2 V.

A. Resolution and FoM

Since the phase output of the WB sensor is determined by its driving frequency, random jitter will translate into random phase noise and degrade the sensor's resolution. To prevent this, the sensors are driven by a low-jitter (1 ps$_{rms}$) frequency reference (SiT8208), which only degrades the sensor's resolution by about 0.5%. Furthermore, the temperature of the sensors was stabilized by mounting them inside a cavity in a large (10 kg) metal block, which, in turn, was placed in a temperature-controlled oven (Vötsch VT7004).

The power spectral densities of both sensors' output bit streams are shown in Fig. 10(a). The sensor's noise floor is dominated by the *RC*-filters' thermal noise. After decimating
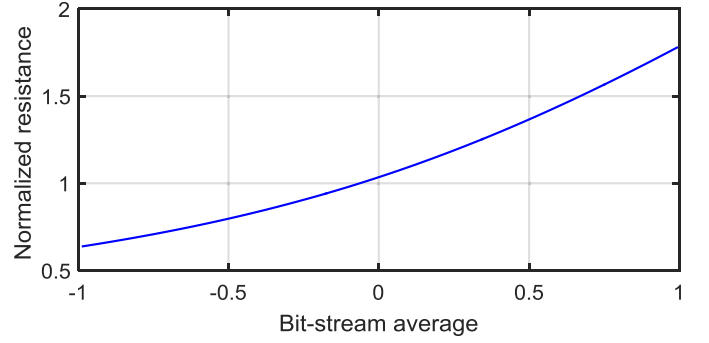
their bit streams at room temperature (RT $\sim$ 25 °C), the sensors' resolution is plotted versus conversion time [Fig. 10(b)]. To suppress the effects of ambient temperature drift, the resolution was determined from a two-sample Allan deviation, i.e., from the difference between two successive measurements. In a 5-ms conversion time (2500 samples), the s-p-poly and the n-poly sensors achieved a resolution of 410 and 880 μK$_{rms}$, respectively. The n-poly resistor exhibits a $1/f$ corner of about 10 Hz, while that of the s-p-poly sensor is below 1 Hz. Since the two sensors are readout in exactly the same way, the $1/f$ noise of the n-poly sensor can be directly attributed to the sensing resistors.

B. Nonlinearity Correction and Calibration

As discussed in Section II-B, the WB sensor's temperature dependence is mainly determined by that of its resistors. Since both the value and the TC of on-chip sensing resistors spread [21], resistor-based temperature sensors usually require a multi-point ($\geq$2) trim to achieve good accuracy, e.g., 0.12 °C with a three-point trim [3].

The accuracy of the proposed WB sensor is also influenced by its nonlinearity, which is due to three factors: 1) the nonlinear temperature dependence of its sensing resistors; 2) the WB's nonlinear resistance-to-phase shift characteristic given by (2); and 3) the nonlinear transfer function of a PD$\Delta\Sigma$M, which is caused by the nonlinearity of its phase demodulator and is referred to as "cosine nonlinearity" [2], [22]. The modulator's nonlinear transfer function is completely deterministic, and can be removed before calibration [2], [23]. Moreover, from (2)

$$R = \frac{1}{2\omega C} \cdot \left(\sqrt{9 \tan^2 (\varphi_{WB}) + 4} - 3 \tan (\varphi_{WB}) \right). \quad (8)$$

So assuming that C and ω are the temperature independent, the resistance-to-phase shift nonlinearity is also fully deterministic. Although (8) assumes that the WB is driven and demodulated by sine waves, the same conclusion can be drawn for the case when square waves are employed.

In our previous work [23], the nonlinearity of the modulator was corrected by a fixed polynomial. In this paper, however, both the nonlinearity of the WB and the modulator are corrected by a fixed seventh-order polynomial. This polynomial is determined from simulation results, assuming ideal readout electronics, temperature-independent WB capacitors,
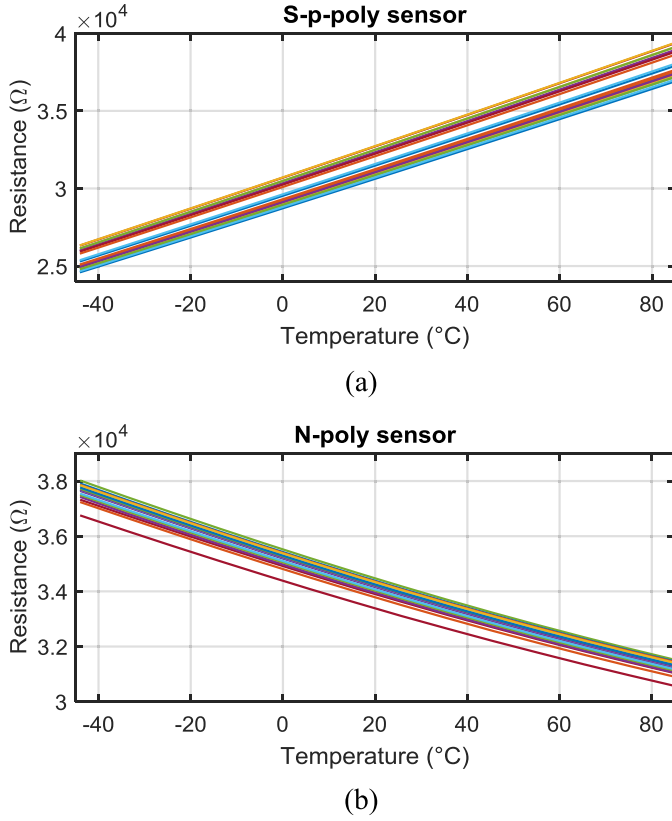
(a)

(b)

Fig. 12. R–T plots of (a) s-p-poly sensor and (b) n-poly sensor in ceramic packages.

(a)

(b)

Fig. 13. Average resistance versus temperature of (a) s-p-poly sensor and (b) n-poly sensor.

and square-wave drive and demodulation signals. The result is shown in Fig. 11, in which resistance (normalized to its value at f_0) is plotted versus the modulator's bit-stream average.

Twenty samples from one wafer in ceramic dual in-line packages were characterized from −45 °C to 85 °C (steps of 10 °C) in a temperature-controlled oven. The actual temperature was established by a calibrated Pt-100 RTD. To partially compensate for the spread of f_0 with process, f_{drive} was set to 562.5 kHz (9 MHz master clock) instead of the nominal 500 kHz. After the aforementioned fixed nonlinearity correction, the extrapolated resistance versus temperature plots (R–T plots) of the s-p-poly and the n-poly sensors are shown in Fig. 12, and the corresponding average R–T plots are shown in Fig. 13. The corresponding first- and second-order TCs agree well, to within a few percent, with the models provided by the foundry, thus validating the nonlinearity correction technique. After first-order linear fit, the remaining nonlinearity, mainly due to the nonlinearity of the sensing resistor's TC, is quite systematic (Fig. 14), and so could be removed by a fixed third-order polynomial obtained by batch calibration. After this systematic nonlinearity correction, the s-p-poly sensor achieves a 3σ inaccuracy of ±0.03 °C, while the n-poly sensor's inaccuracy is about ±0.3 °C as shown in Fig. 15. Benefiting from the more complete nonlinearity correction, the accuracy of the s-p-poly sensor is 2 × better than that reported in our previous work [23].

To reduce calibration costs, the number of calibration temperatures should be reduced. So rather than doing a first-order fit based on data obtained at multiple temperature points,
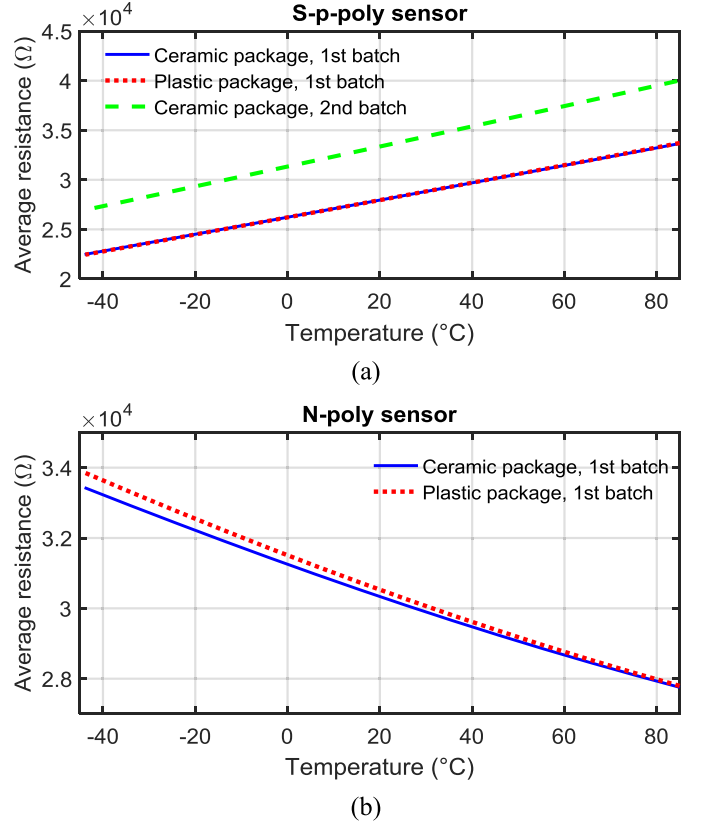
a simpler two-point calibration can be done. This result in only a slight loss of accuracy: when calibrated at −15 °C and 65 °C, the s-p-poly sensor achieves a 3σ inaccuracy of ±0.05 °C.

C. Single-Point Calibration

Serendipitously, the TC and the RT resistance (R_0) of the s-p-poly sensor were found to be highly correlated, as shown in Fig. 16(a). By exploiting this correlation, a 3σ inaccuracy of ±0.2 °C could be achieved after a single-point calibration, as shown in Fig. 16(c). Unfortunately, this correlation is much weaker for n-poly sensor [Fig. 16(b)], and the 3σ inaccuracy after a single-point calibration is only ±0.6 °C.

D. Plastic Packaging

In production, low-cost plastic packages are preferred over ceramic packages. However, the accompanying mechanical stress [24] impacts the sensor's accuracy. Because of the metal-like properties of silicided poly resistors, their stress sensitivity is much less than that of non-silicided poly resistors. The average R-T plot of 12 sensors produced in the same batch is shown in Fig. 13. Compared to the ceramic packaged chips, both the TC and R_0 of the n-poly resistors in plastic packages change significantly, while those of the s-p-poly resistors do not.

However, compared to ceramic packaged devices, a shift was observed in the TC-R_0 correlation of the s-p-poly sensors. Even based on the limited number of samples, the correlation

	This Work	JSSC15 [4]	JSSC15 [3]	JSSC13 [1]	JSSC17 [6]	TIE17 [9]
Sensor type	Resistor WB	Resistor WhB	Resistor WB	MEMS Resistor	MEMS Resonator	BJT
Tech (μm)	0.18	0.18	0.18	0.18	0.18	0.7
Area (mm^2)	0.72	0.43	0.09	0.18	0.54	1.5
Power (mW)	0.16	0.065	0.031	13	19	0.16
Temp. Range (°C)	−40—85	−40—125	−40—85	−40—85	−40—105	−40—130
Resolution (mK)	0.41	10	2.8	0.1	0.02	3
T_{conv} (ms)	5	0.1	32	100	5	1.8
Trim point	2[a]	2[b]	3	6	--	1
Inaccuracy (3σ)	±30mK	±400mK[c]	±120mK[c]	--	--	±300mK
Res. FoM (pJ·K^2)	0.13	0.65	8	13[d]	0.04[d]	3.2

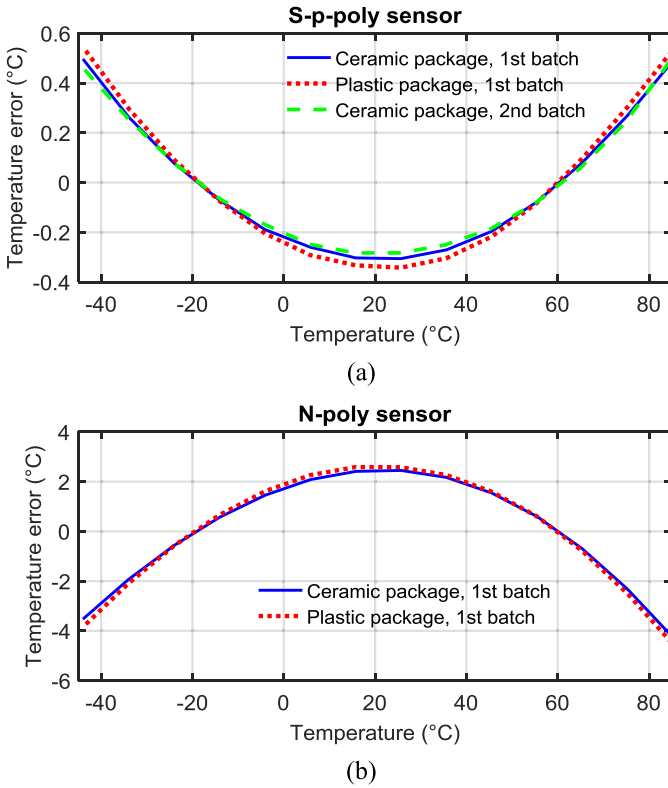[a] 1st-order fit. [b] 1-point trim with fixed 1st-order fit. [c] Min/Max. [d] MEMS die + CMOS readout IC.

Fig. 14. Systematic temperature nonlinearity of (a) s-p-poly sensor and (b) n-poly sensor after a first-order fit.
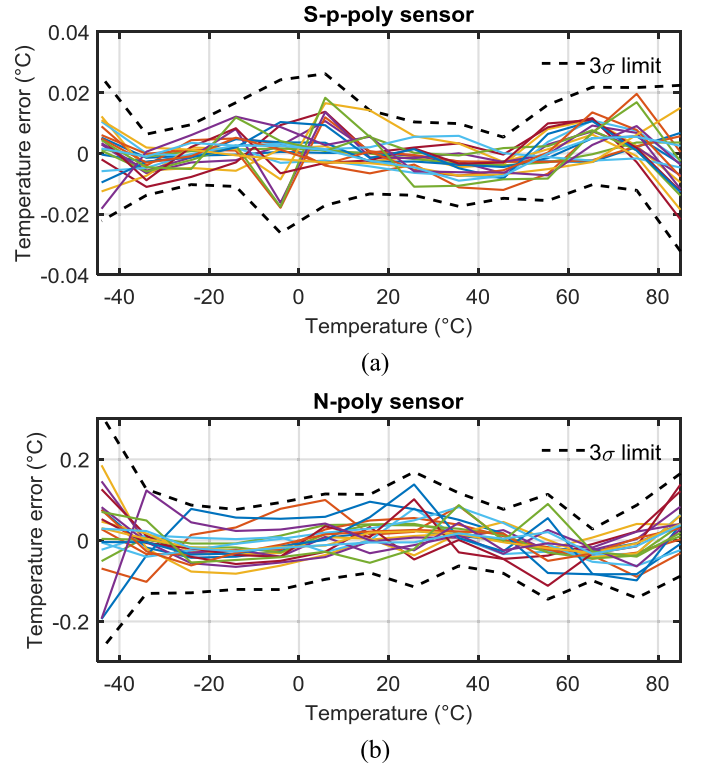

Fig. 15. Inaccuracy of (a) s-p-poly sensor and (b) n-poly sensor after a first-order fit and systematic nonlinearity removal.

also appears to be weaker, as shown by the presence of an outlier in Fig. 16(a). After a two-point calibration, however, the change in their systematic nonlinearity is less than 0.05 °C (Fig. 14). After a packaging-specific systematic nonlinearity correction, the sensor achieves a 3σ inaccuracy of ±0.2 °C, as shown in Fig. 17, mainly due to the outlier.

E. Batch-to-Batch Spread

To verify the effect of batch-to-batch spread on the s-p-poly sensor's inaccuracy, 12 devices from a different batch (fabricated a few months after the first batch) were characterized in ceramic packages. As shown in Fig. 13, however, the center frequency f_0, and hence the extrapolated resistance of the s-p-poly sensors then shifted by about 16%. To maximize the sensors' resolution, this resistance shift was compensated by reducing f_{drive} by 16% during characterization. The sensor's extrapolated TC-R_0 relationship is shown in Fig. 16. Despite the significant shift in f_0, the linear correlation discussed in Section IV-C is still valid. The s-p-poly sensor achieves an estimated 3σ inaccuracy of ±0.3 °C after a correlation-assisted single-point calibration. After an individual first-order fit, the maximum difference in the systematic nonlinearity of the two batches is 0.04 °C from −40 °C to 85 °C (Fig. 14).
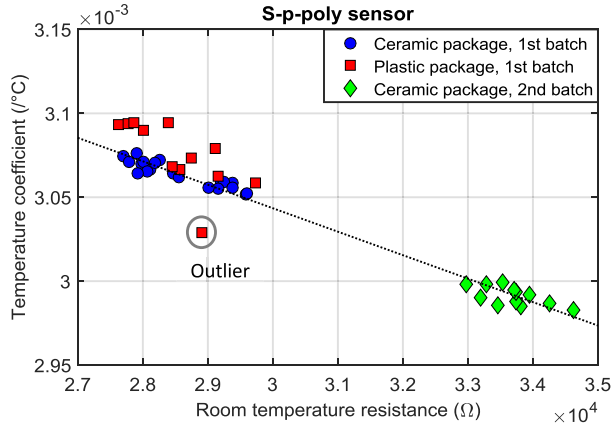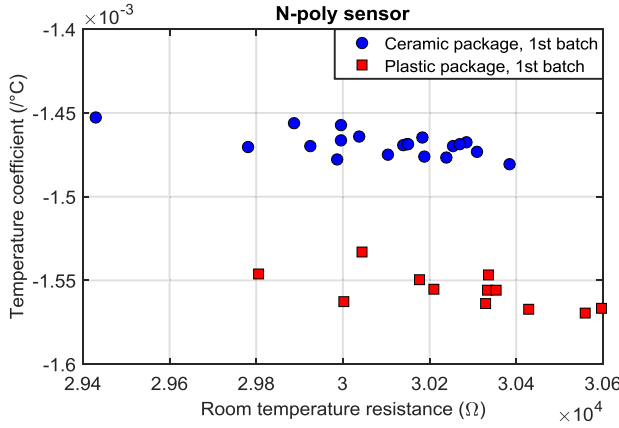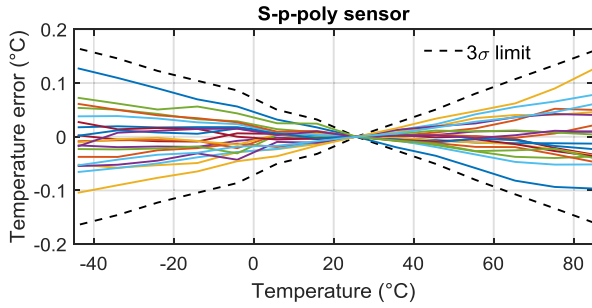
Fig. 16. Correlation between R_0 and its TC for (a) s-p-poly resistor and (b) n-poly resistor. (c) Inaccuracy of s-p-poly sensor after a correlation-assisted one-point calibration (ceramic packaged, first batch).

F. Comparison to Previous Work

The performance of the s-p-poly sensor's is summarized in Table II and compared to that of other high-resolution energy-efficient temperature sensors. It achieves an energy efficiency of 0.13 pJ·K², which is 5 × better than the state of the art for CMOS sensors [4], and is close to that of MEMS-based sensors [7]. When packaged in ceramic, the sensor achieves an inaccuracy of ±0.03 °C (3σ) after a first-order fit followed by a fixed systematic nonlinearity correction, which is the best reported for a CMOS resistor-based temperature sensor. It also achieves ±0.2 °C (3σ) after a single-point calibration, which is comparable to that of most BJT-based sensors [16].
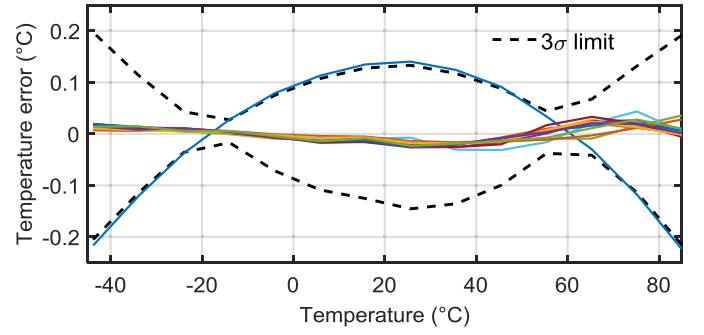

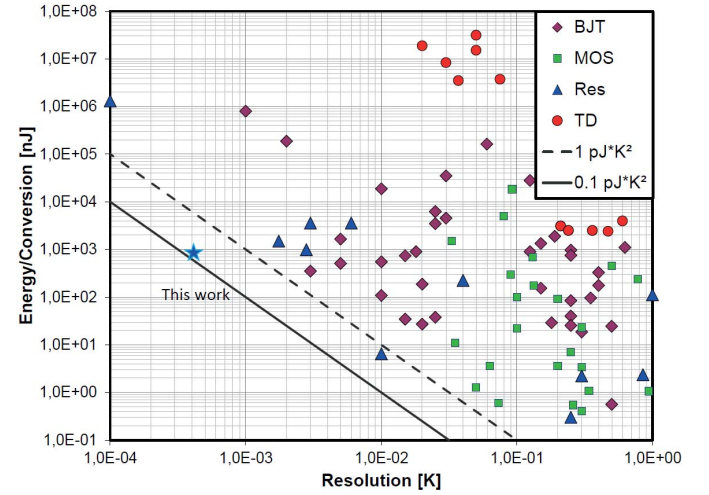Fig. 17. Inaccuracy of plastic packaged s-p-poly sensor after a first-order fit and systematic nonlinearity removal.

Fig. 18. Energy per conversion versus resolution for CMOS smart temperature sensors [16].

V. CONCLUSION

A resistor-based smart temperature sensor for the temperature compensation of MEMS/quartz frequency references has been implemented in a standard 0.18-μm CMOS technology. It is based on a WB RC filter, whose output phase is digitized by a continuous-time PD$\Delta\Sigma$M. Mainly due to the high TC and low $1/f$ noise of silicided poly resistors, the sensor achieves a 410-μK resolution in a 5-ms conversion time, and a resolution FoM of 0.13 pJ·K². The sensor has been characterized over two batches and packages (ceramic/plastic). When packaged in ceramic, it achieves an inaccuracy of ±0.2 °C (3σ) from −40 °C to 85 °C after a single-point calibration. After a first-order fit and a systematic nonlinearity correction, this can be reduced to ±0.03 °C (3σ) over the same temperature range. These results demonstrate that silicided poly resistors are suitable for realizing the high-resolution and energy-efficient sensors required for the temperature compensation of precision frequency references.

References

[1] M. H. Perrott *et al.*, "A temperature-to-digital converter for a MEMS-based programmable oscillator with < ±0.5-ppm frequency stability and < 1-ps integrated jitter," *IEEE J. Solid-State Circuits*, vol. 48, no. 1, pp. 276–291, Jan. 2013.

[2] M. Shahmohammadi, K. Souri, and K. A. A. Makinwa, "A resistor-based temperature sensor for MEMS frequency references," in *Proc. ESSCIRC*, Sep. 2013, pp. 225–228.

[3] P. Park, D. Ruffieux, and K. A. A. Makinwa, "A thermistor-based temperature sensor for a real-time clock with ±2 ppm frequency stability," *IEEE J. Solid-State Circuits*, vol. 50, no. 7, pp. 1571–1580, Jul. 2015.

[4] C. H. Weng, C. K. Wu, and T. H. Lin, "A CMOS thermistor-embedded continuous-time delta-sigma temperature sensor with a resolution FoM of 0.65 pJ °C^2," *IEEE J. Solid-State Circuits*, vol. 50, no. 11, pp. 2491–2500, Nov. 2015.

[5] K. A. Sankaragomathi, J. Koo, R. Ruby, and B. P. Otis, "A ±3 ppm 1.1 mW FBAR frequency reference with 750 MHz output and 750 mV supply," in *IEEE Int. Solid-State Circuits Conf. (ISSCC) Dig. Tech. Papers*, Feb. 2015, pp. 1–3.

[6] D. Ruffieux *et al.*, "A 3.2 × 1.5 × 0.8 mm^3 240 nA 1.25-to-5.5 V 32 kHz-DTCXO RTC module with an overall accuracy of ±1 ppm and an all-digital 0.1 ppm compensation-resolution scheme at 1 Hz," in *IEEE Int. Solid-State Circuits Conf. (ISSCC) Dig. Tech. Papers*, Feb. 2016, pp. 208–209.

[7] M. H. Roshan *et al.*, "A MEMS-assisted temperature sensor with 20-μK resolution, conversion rate of 200 S/s, and FOM of 0.04 pJK^2," *IEEE J. Solid-State Circuits*, vol. 52, no. 1, pp. 185–197, Jan. 2017.

[8] M. A. P. Pertijs, K. A. A. Makinwa, and J. H. Huijsing, "A CMOS smart temperature sensor with a 3σ inaccuracy of ±0.55 °C from −55 °C to 125 °C," *IEEE J. Solid-State Circuits*, vol. 40, no. 12, pp. 2805–2815, Dec. 2005.

[9] G. Wang, A. Heidari, K. A. A. Makinwa, and G. C. M. Meijer, "An accurate BJT-based CMOS temperature sensor with duty-cycle-modulated output," *IEEE Trans. Ind. Electron.*, vol. 64, no. 2, pp. 1572–1580, Feb. 2017.

[10] B. Yousefzadeh, S. H. Shalmanym, and K. A. A. Makinwa, "A BJT-based temperature-to-digital converter with ±60 mK (3σ) inaccuracy from −55 °C to +125 °C in 0.16 μm CMOS," *IEEE J. Solid-State Circuits*, vol. 52, no. 4, pp. 1044–1052, Apr. 2017.

[11] K. Souri, Y. Chae, F. Thus, and K. Makinwa, "A 0.85 V 600 nW all-CMOS temperature sensor with an inaccuracy of ±0.4 °C (3σ) from −40 to 125 °C," in *IEEE Int. Solid-State Circuits Conf. (ISSCC) Dig. Tech. Papers*, Feb. 2014, pp. 222–223.

[12] T. Anand, K. A. A. Makinwa, and P. K. Hanumolu, "A VCO based highly digital temperature sensor with 0.034 °C/mV supply sensitivity," *IEEE J. Solid-State Circuits*, vol. 51, no. 11, pp. 2651–2663, Nov. 2016.

[13] X. Tang, K. P. Pun, and W. T. Ng, "A 0.9 V 5 kS/s resistor-based time-domain temperature sensor in 90 nm CMOS with calibrated inaccuracy of −0.6 °C/0.8 °C from −40 °C to 125 °C," in *Proc. IEEE Asian Solid-State Circuits Conf.*, Nov. 2013, pp. 169–172.

[14] C. P. L. van Vroonhoven, D. d'Aquino, and K. A. A. Makinwa, "A thermal-diffusivity-based temperature sensor with an untrimmed inaccuracy of ±0.2 °C (3σ) from −55 °C to 125 °C," in *IEEE Int. Solid-State Circuits Conf. (ISSCC) Dig. Tech. Papers*, Feb. 2010, pp. 314–315.

[15] U. Sönmez, F. Sebastiano, and K. A. A. Makinwa, "Compact thermal-diffusivity-based temperature sensors in 40-nm CMOS for SoC thermal monitoring," *IEEE J. Solid-State Circuits*, vol. 52, no. 3, pp. 834–843, Mar. 2017.

[16] K. A. A. Makinwa. *Smart Temperature Sensor Survey*. [Online]. Available: http://ei.ewi.tudelft.nl/docs/TSensor_survey.xls

[17] H. C. de Graaff and M. T. M. Huybers, "1/f noise in polycrystalline silicon resistors," *J. Appl. Phys.*, vol. 54, no. 5, pp. 2504–2507, 1983.

[18] E. Vereshchagina, R. A. M. Wolters, and J. G. E. Gardeniers, "The development of titanium silicide–boron-doped polysilicon resistive temperature sensors," *J. Micromech. Microeng.*, vol. 21, no. 10, p. 105022, 2011.

[19] P. Li, J. Peng, and D. W. Zhang, "The study on metal-insulator-metal capacitor performance improvement," in *Proc. ICSICT*, Oct. 2014, pp. 1–3.

[20] K. Nam, S.-M. Lee, D. K. Su, and B. A. Wooley, "A low-voltage low-power sigma-delta modulator for broadband analog-to-digital conversion," *IEEE J. Solid-State Circuits*, vol. 40, no. 9, pp. 1855–1864, Sep. 2005.

[21] R. K. Waits, "Silicide resistors for integrated circuits," *Proc. IEEE*, vol. 59, no. 10, pp. 1425–1429, Oct. 1971.

[22] S. M. Kashmiri, S. Xia, and K. A. A. Makinwa, "A temperature-to-digital converter based on an optimized electrothermal filter," *IEEE J. Solid-State Circuits*, vol. 44, no. 7, pp. 2026–2035, Jul. 2009.

[23] S. Pan, Y. Luo, S. H. Shalmany, and K. A. A. Makinwa, "A resistor-based temperature sensor with a 0.13 pJ·K^2 resolution FOM," in *IEEE Int. Solid-State Circuits Conf. (ISSCC) Dig. Tech. Papers*, Feb. 2017, pp. 158–159.

[24] A. Hastings, *The Art of Analog Layout*. Englewood Cliffs, NJ, USA: Prentice-Hall, 2001.
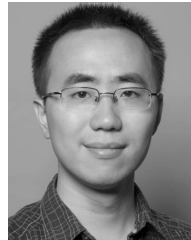
Sining Pan (S'16) was born in China, in 1991. He received the B.Sc. degree in electronic engineering from Tsinghua University, Beijing, China, in 2013, and the M.Sc. (*cum laude*) degree in electrical engineering from the Delft University of Technology, Delft, The Netherlands, in 2016, where he is currently pursuing the Ph.D. degree, focusing on the design of energy-efficient CMOS temperature sensors.

Yanquan Luo was born in Xiaguan, China. She received the B.S. degree in microelectronics from Fudan University, Shanghai, China, in 2013, and the M.S. degree in microelectronics from the Delft University of Technology, Delft, The Netherlands, in 2015. She is currently pursuing the Ph.D. degree at the University of Ulm, Ulm, Germany.

Her current research interest is high resolution power-efficient data converter design.

Saleh Heidary Shalmany (S'12) received the B.Sc. degree in electrical engineering from Tehran University, Tehran, Iran, in 2008, the M.Sc. (*cum laude*) degree in electrical engineering from TU Delft, Delft, The Netherlands, in 2010. From 2011 to 2016, he pursued his Ph.D. at TU Delft, in collaboration with Infineon Technologies, Villach, Austria.

From 2010 to 2011, he was a Researcher with TU Delft and NXP Semiconductor, Leuven, Belgium. He joined Broadcom, Bunnik, The Netherlands in 2016 and subsequently SiTime, Delft, The Netherlands in 2017. His current research interests include analog and mixed-signal circuits, data converters, and low-power sensor interfaces.

Mr. Heidary Shalmany was a recipient of the Huygens Scholarship during 2008–2010 and the IEEE SSCS Predoctoral Achievement Award in 2015. He is also a co-recipient of the VLSI-2016 Best Student Paper Award.

Kofi A. A. Makinwa (M'97–SM'05–F'11) received the B.Sc. and M.Sc. degrees from Obafemi Awolowo University, Ife, Nigeria, in 1985 and 1988, respectively, the M.E.E. degree from the Philips International Institute, Eindhoven, The Netherlands, in 1989, and the Ph.D. degree from Delft University of Technology, Delft, The Netherlands, in 2004.

From 1989 to 1999, he was a Research Scientist with Philips Research Laboratories, Eindhoven, The Netherlands, where he worked on interactive displays and digital recording systems. In 1999, he joined the Delft University of Technology, where he is currently an Antoni van Leeuwenhoek Professor and the Head of the Microelectronics Department. He has authored 15 books and over 200 technical papers, and holds 25 patents. His current research interests include the design of precision mixed-signal circuits, sensor interfaces, and smart sensors.

Dr. Makinwa is the Analog Subcommittee Chair of the International Solid-State Circuits Conference (ISSCC). He is also on the program committees of the VLSI Symposium, the European Solid-State Circuits Conference (ESSCIRC), and the Advances in Analog Circuit Design workshop. He has been a Guest Editor of the *Journal of Solid-State Circuits* (JSSC) and a Distinguished Lecturer of the IEEE Solid-State Circuits Society. For his doctoral research, he received the 2005 Simon Stevin Gezel Award from the Dutch Technology Foundation. He was a co-recipient of 15 best paper awards from the JSSC, ISSCC, VLSI, ESSCIRC and Transducers, among others. At the 60th anniversary of ISSCC, he was recognized as a top-10 contributor. He is an alumnus of the Young Academy of the Royal Netherlands Academy of Arts and Sciences and an Elected Member of the IEEE Solid-State Circuits Society AdCom, the society's governing board.